

1 scGAE: topology-preserving dimensionality 2 reduction for single-cell RNA-seq data using graph 3 autoencoder

4 Zixiang Luo^{1,+}, Chenyu Xu^{2,+}, Zhen Zhang^{3,*}, and Wenfei Jin^{1,*}

5 ¹Department of Biology, Southern University of Science and Technology, Shenzhen 518055, China

6 ²Department of Electric Engineering, Iowa state university, IA, 50011, USA

7 ³Department of Mathematics, Southern University of Science and Technology, Shenzhen 518055, China

8 *jinwf@sustech.edu.cn (WJ) or zhangz@sustech.edu.cn (ZZ)

9 +these authors contributed equally to this work

10 ABSTRACT

Dimensionality reduction is crucial for the visualization and interpretation of the high-dimensional single-cell RNA sequencing (scRNA-seq) data. However, preserving topological structure among cells to low dimensional space remains a challenge. Here, we present the single-cell graph autoencoder (scGAE), a dimensionality reduction method that preserves topological structure in scRNA-seq data. scGAE builds a cell graph and uses a multitask-oriented graph autoencoder to preserve topological structure information and feature information in scRNA-seq data simultaneously. We further extended scGAE for scRNA-seq data visualization, clustering, and trajectory inference. Analyses of simulated data showed that scGAE accurately reconstructs developmental trajectory and separates discrete cell clusters under different scenarios, outperforming recently developed deep learning methods. Furthermore, implementation of scGAE on empirical data showed scGAE provided novel insights into cell developmental lineages and preserved inter-cluster distances.

12 Introduction

13 Single-cell RNA sequencing (scRNA-seq) is an ideal approach for investigating cell-cell variation. Conventional dimensionality
14 reduction techniques such as principal component analysis (PCA) and t-Distributed Stochastic Neighbor Embedding (t-SNE)¹
15 were implemented on scRNA-seq data for visualization and downstream analyses, significantly increasing our understanding
16 of cellular heterogeneity and development progress. The recent emergence of massively parallel scRNA-seq such as droplet
17 platforms enabled interrogation of millions of cells in complex biological systems²⁻⁵, which provide a fantastic potential for
18 dissection of tissue and cellular microenvironment, identification of rare/new cell types, inference of developmental lineages,
19 and elucidation of the mechanism of cellular response to stimulations⁶. However, the data generated by massively parallel
20 scRNA-seq are of high dropout and high noise with complex structure, which posed a series of challenges on dimensionality
21 reduction. Particularly, it is a big challenge to preserve the complex topological structure among cells.

22 Many dimensionality reduction methods have been developed or introduced for scRNA-seq data analyses in the past
23 several years. Recently developed competitive methods include DCA⁷, SCVI⁸, scDeepCluster⁹, PHATE¹⁰, SAUCIE¹¹, and
24 Ivis¹². Among them, deep learning showed the greatest potentials. For instance, DCA, scDeepCluster, Ivis, and SAUCIE
25 adapted the autoencoder to denoise, visualize and cluster the scRNA-seq data. However, these deep learning-based models only
26 embedded the distinct cell features while ignoring the cell-cell relationships, which limited their ability to reveal the complex
27 topological structure among cells and made them difficult to elucidate the developmental trajectory. The recently proposed
28 graph autoencoder¹³ is very promising as it preserves the long-distance relationships among data in a latent space. In this study,
29 we developed the single-cell graph autoencoder (scGAE). It improved the graph autoencoder to preserving global topological
30 structure among cells. We further extended the scGAE for visualization, trajectory inference, and clustering. Analyses of
31 simulated data and empirical data showed that scGAE outperformed the other competitive methods.

32 Results

33 The Model architecture of scGAE

34 scGAE combines the advantage of the deep autoencoder and graphical model to embed the topological structure of high-
35 dimensional scRNA-seq data to a low-dimensional space (Fig1). After getting the normalized count matrix, scGAE builds the
36 adjacency matrix among cells by K-nearest-neighbor algorithm. The encoder maps the count matrix to a low-dimensional latent

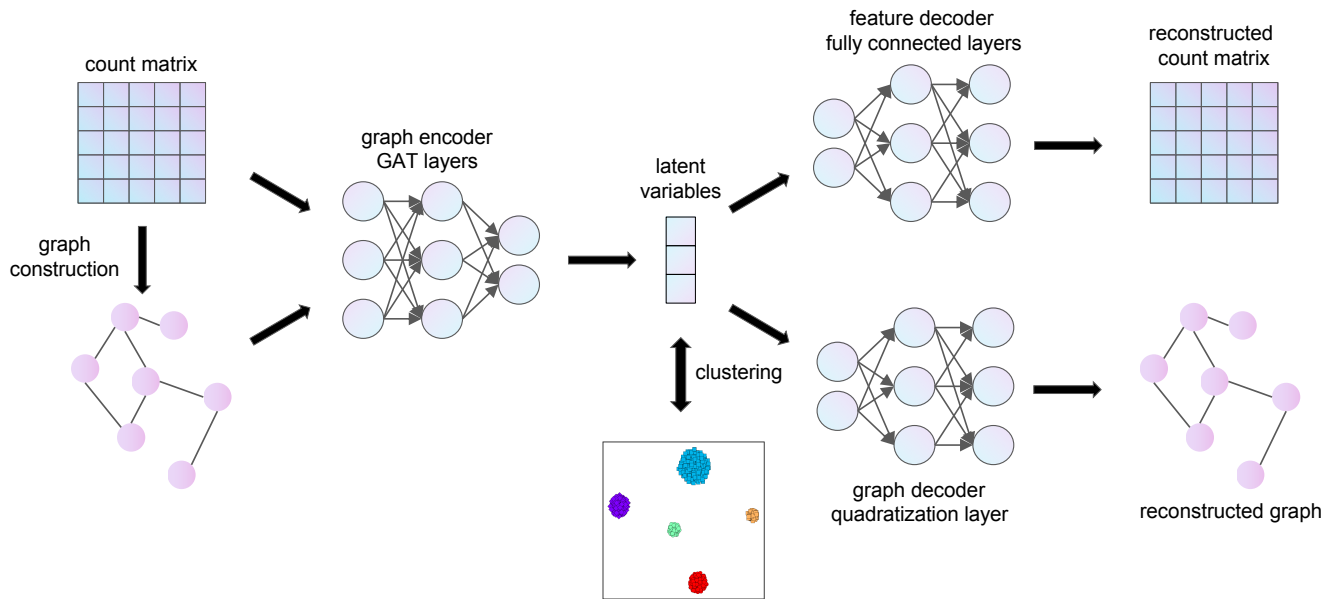


Figure 1. The Model architecture of scGAE. The normalized count matrix represents the gene expression level in each cell. The adjacency matrix is constructed by connecting each cell to its K nearest neighbors. The encoder takes the count matrix and the adjacency matrix as inputs and generates low-dimensional latent variables. The feature decoder reconstructs the count matrix. The graph decoder reconstructs the adjacency matrix. Clustering is performed on the latent variables.

37 space by graph attentional layers¹⁴. scGAE decodes the embedded data with a feature decoder and a graph decoder. The feature
38 decoder reconstructs the count matrix to preserve the feature information; The graph decoder recovers the adjacency matrix and
39 preserves the topological structure information. It decodes the embedded data to the spaces with the same dimension as original
40 data by minimizing the distance between the input data and the reconstructed data (see Methods). We use deep clustering to
41 learn the data embedding and do cluster assignment simultaneously¹⁵, generating a clustering-friendly latent representation.
42 The implementation and usage of scGAE can be found on Github: <https://github.com/ZixiangLuo1161/scGAE>.

43 Visualization of scGAE embedded data and comparison to other methods

44 To systematically evaluate the performance of scGAE, we summarized four representative scenarios (scenario1: cells in
45 continuous differentiation lineages; scenario2: cells in differentiation lineages where cells concentrate at the center of each
46 branch; scenario3: distinct cell populations with apparent differences; and scenario4: distinct cell populations with small
47 population differences) (Fig2 left). We used Splatter¹⁶ and PROSSTT¹⁷ to simulate scRNA-seq data for scenario1, scenario2,
48 scenario3, and scenario4. The latent embedding inferred by scGAE was visualized by tSNE. In scenario1 and scenario2, scGAE
49 almost entirely reproduced the differentiation lineages (Fig2a, 2b), while other methods only revealed some local structures and
50 failed to exhibit the overall structure of simulated data (Fig2a, 2b). The results of tSNE and SAUCIE exhibited distinct clusters
51 but lost lineage relationship in scenario2 (Fig2b). In scenario3 and scenario4, scGAE almost perfectly preserved the compact
52 cell clusters and inter-cluster distances in the simulated data, while the clusters inferred by other methods are dispersed, and the
53 topological structure among these clusters was not preserved (Fig2c, 2d, Supplemental figure 1). Only scGAE separated all the
54 clusters while the other methods mixed different types of cells when the differences between clusters are small (Fig 2d). Based
55 on these observations, scGAE perfectly reproduced the differentiation lineages and distinct clusters in the simulated data (Fig2),
56 indicating scGAE outperforms other competitive methods in restoring the relationship between cells.

57 Trajectory inference and cell clustering based on scGAE embedded data

58 We further quantitatively evaluated the performance of scGAE for trajectory inference tasks. The scGAE and several other
59 competitive methods were used to perform dimensionality reduction on the simulated lineages (simulated by PROSSTT)
60 (scenario1 and 2). We conducted trajectory inference on these embedded data using DPT¹⁸. The Kendall correlation coefficient¹⁹
61 between the inferred trajectories and the ground truth was calculated to measure their similarity. The results showed that
62 scGAE and SCVI better recovered the original trajectory than the other competitive methods on both scenario1 and 2 (Fig3a,
63 Fig3b). Next, we evaluated the performance of scGAE on cell clustering tasks. Simulated data with cell clusters (simulated by
64 Splatter) (scenario3 and 4) were analyzed by scGAE and other competitive methods. We performed Louvain clustering on

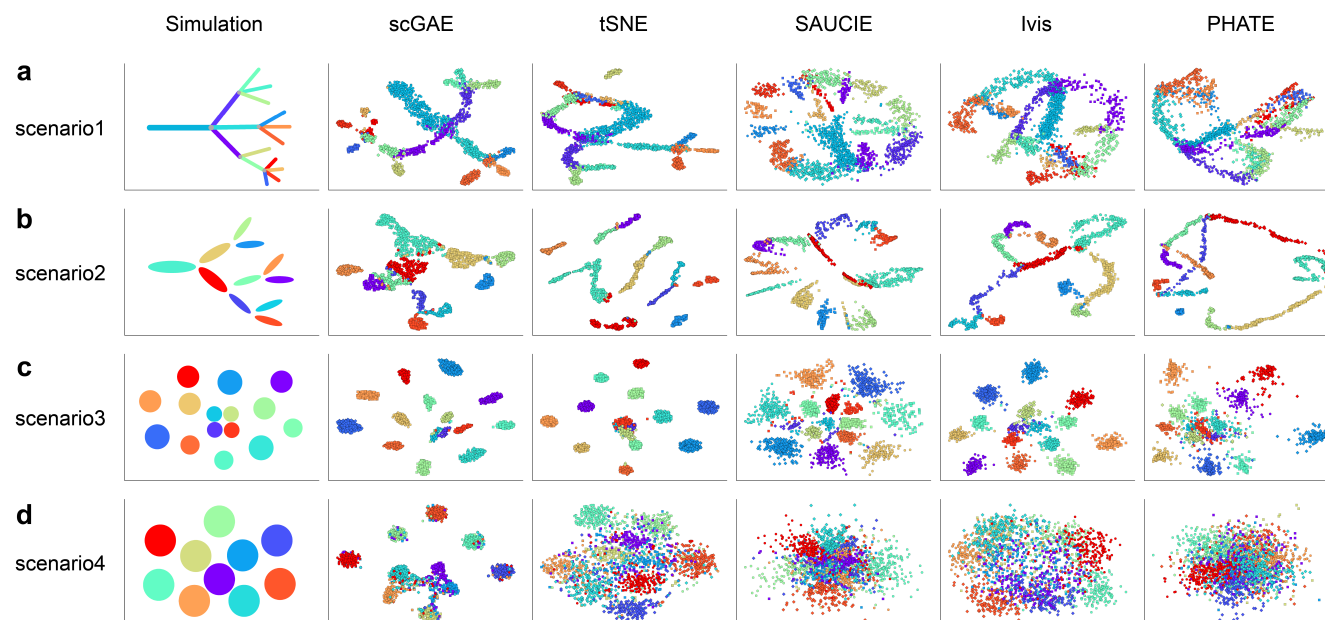


Figure 2. Visualization of the four simulated datasets by scGAE, tSNE, SAUCIE, Ivis, and PHATE. Each color represents a cell subpopulation in the simulated dataset. (a) scenario1: cells in continuous differentiation lineages. (b) scenario2: cells in differentiation lineages where cells concentrate at the center of each branch. (c) scenario3: distinct cell populations with apparent population differences. (d) scenario4: distinct cell populations with small population differences.

65 these embedded data. Normalized mutual information (NMI) was used to measure the difference between inferred clusters
 66 and ground truth. The results showed that scGAE was the best among these methods (Fig3c, Fig3d). Although SCVI is the
 67 second-best performed for trajectory inference (Fig3a, Fig3b), it is the worst performed for cell clustering (Fig3c, Fig3d). On
 68 the other hand, PCA is the second-best method for cell clustering (Fig3c, Fig3d), while it does not perform well for trajectory
 69 inference. Overall, scGAE performed best for both trajectory inference and cell clustering.

70 **scGAE identified novel subpopulations that shaped hematopoietic lineage relationship**

71 Single cell analysis of hematopoietic stem and progenitor cells (HSPCs) have significantly increased our understanding of the
 72 early cell subpopulations and developmental trajectory during hematopoiesis^{5,20-25}. We further used scGAE to analyze HSPCs
 73 scRNA-seq data from our previous study⁵ (Fig4a). We found the previous identified Basophil/Eosinophil/Mast progenitors
 74 (Ba/Eo/MaP) has been classified into multiple subpopulations (Fig4b). It indicates that the cells in Ba/Eo/MaP may have
 75 different differentiation potentials at early phase. While the other competitive methods did not identify the subpopulations in
 76 Ba/Eo/MaP (Supplemental figure 2), supporting scGAE has the highest statistical power to identify the substructure in the
 77 scRNA-seq data.

78 **scGAE preserved topological structure among human pancreatic cells populations**

79 The function of the pancreas hinges on complex interactions among distinct cell types and cell populations. We re-analyzed
 80 the scRNA-seq data of human pancreatic cells from Baron et al.²⁶. Although the pancreatic cell subpopulations identified
 81 by scGAE are the same as the original study, we found the distances and topological structures among cell types inferred by
 82 scGAE better fit our knowledge (Fig4c). For instance, the activated stellate and quiescent stellate showed similar expression
 83 profiles and are very close to each other²⁷, which is recovered by scGAE while not recovered by other methods (Fig4d and
 84 Supplemental figure 2). scGAE also preserved the short distance between two ductal subtypes, while other methods did not
 85 (Fig4d and Supplemental figure 2). Overall, scGAE preserved the topological structure among different cell populations, which
 86 greatly benefit our understanding of the cellular relationships.

87 **Discussion**

88 Because of the high noises of scRNA-seq data and complicated cellular relationships, preserving the topological structure of
 89 scRNA-seq data in low-dimensional space is still a challenge. We proposed scGAE which is a promising topology-preserving
 90 dimensionality reduction method. It generates a low-dimensional representation that better preserves both the global structure

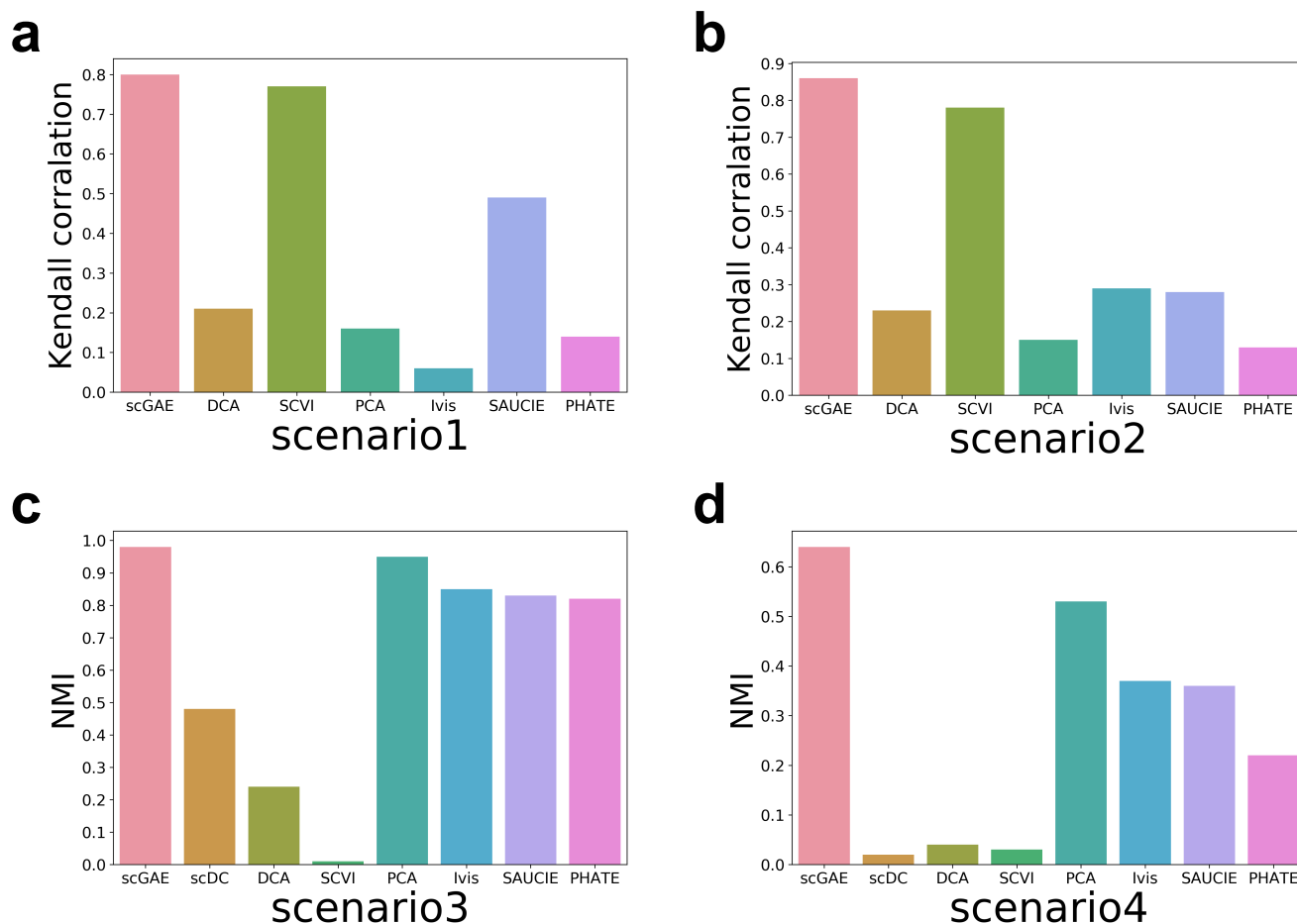


Figure 3. Quantitative evaluation of scGAE and several other competitive methods on clustering and trajectory inference tasks. In scenario1 (a) and scenario2 (b), the Kendall correlation between the ground truth and inferred trajectory was calculated. In scenario3 (c) and scenario4 (d), the normalized mutual information (NMI) measures the difference between the ground truth and the inferred clusters.

91 and local structure of the high-dimensional scRNA-seq data. The key innovation of scGAE is to embed the structure information
 92 and feature information simultaneously using a multitask graph autoencoder. It is suitable for analyzing the data both in
 93 lineages and clusters. The learned latent representation benefits various downstream analyses, including clustering, trajectory
 94 inference, and visualization. The analyses on both simulated data and empirical data suggested scGAE accurately preserved the
 95 topological structures of data.

96 As the first study adapting graph autoencoder for dimensionality reduction of scRNA-seq data, this approach is likely
 97 to be significantly improved in the future. Firstly, because the complex data structure is hard to be directly embedded into
 98 two-dimensional space by graph autoencoder, we embedded the scRNA-seq data into an intermediate dimension and used
 99 tSNE to visualize the embedded data into a two-dimensional space. However, the tSNE focuses more on local information, and
 100 it sometimes fails to correctly recover the global structure, which may distort the topological structure in the data. A better
 101 visualization method is needed to preserve the topological structure of scRNA-seq data. Secondly, the graph in scGAE is
 102 constructed by the K-nearest neighbor (KNN) algorithm that relies on a predefined parameter K. However, the optimal K varies
 103 among different datasets and different parts of a dataset. Constructing an optimal graph is challenging due to the difficulty in
 104 determining a suitable K, which could be our potential future endeavors.

105 Methods

106 Joint graph autoencoder

The graph autoencoder is a type of artificial neural network for unsupervised representation learning on graph-structured data¹³. The graph autoencoder often has a low-dimensional bottleneck layer so that it can be used as a model for dimensionality

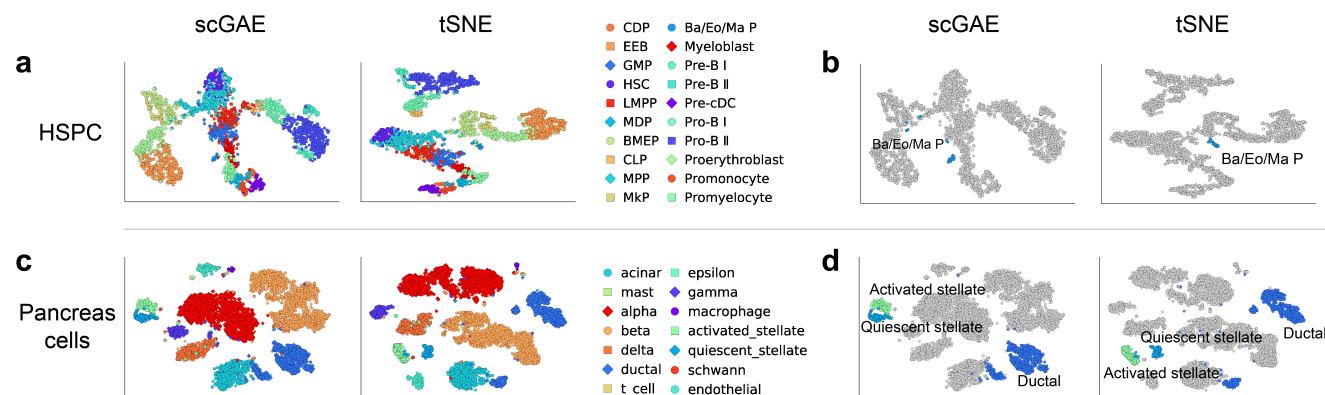


Figure 4. Analyses of two real datasets. (a) Visualization of HSPC cells by scGAE and tSNE (b) scGAE identified the multiple subpopulations in previous reported Ba/Eo/MaP. (c) Visualization of pancreases cells by scGAE and tSNE. (d) The close distance between two stellate states and the short distance between ductal subtypes recovered by scGAE.

reduction. Let the inputs be single-cell graphs of node matrices X and adjacency matrices A . In our joint graph autoencoders²⁸, there is one encoder E for the whole graph and two decoders D_X and D_A for nodes and edges respectively. In practice, we first encode the input graph into a latent variable $h = E(X, A)$, and then we decode h into the reconstructed node matrix $X_r = D_X(h)$ and the reconstructed adjacency matrix $A_r = D_A(h)$. The objective of learning process is to minimize the the reconstruction loss

$$L_r = \lambda \|X - X_r\|_2^2 + (1 - \lambda) \|A - A_r\|_2^2,$$

107 where the weight λ is a hyper-parameter. In our experiments, λ is set to be 0.6.

108 We used the Python package Spektral²⁹ to implement our model. There are many types of graph neural networks that
 109 can be used as the encoder or decoder. Hereby, to extract the features of a node with the aid of its neighbors, we apply graph
 110 attention layers as default in the encoder. Other graph neural networks such as GCN³⁰, GraphSAGE³¹ and TAGCN³² can also
 111 be implemented as the encoder in scGAE. The feature decoder D_X is a four-layer fully connected neural network with 64, 256,
 112 512 nodes in hidden layers.

The edge decoder consists of a fully connected layer followed by the composition of quadratization and activation:

$$A_r = D_A(h) = \sigma(ZZ^T),$$

113 where $Z = \sigma(Wh)$ arises as an output of a fully connected layer with the weight matrix W , and $\sigma(x) = \max(0, x)$ is the rectified
 114 linear unit.

115 Deep-clustering embedding

Motivated by Yang et al³³, we use a two-stage method. The first stage is to pre-train scGAE by minimizing L_r . The resulting
 neural network parameters are set as the initialization of the second stage, which we call alter-training. The loss function in the
 alter-training stage compromises both reconstruction error L_r and clustering cost $L_c = L_c(h, \mu)$:

$$L = L_r + \gamma L_c,$$

116 where μ is a collection of clustering centroids, and γ is a hyper-parameter set as 2.5 in our experiments.

117 The alter-training consists of doing the following two steps alternately:

- 118 1. Given a collection of clustering centroids μ , update network parameters by minimizing L ;
- 119 2. Compute the embedded data h using the updated network, and do clustering in the embedded space to obtain new
 120 centroids μ ;

121 In experiments, we use the pre-trained network to generate the initial embedded data which are clustered to obtain the initial
 122 centroids by Louvain³⁴. There are various choices for the loss L_c and the clustering algorithm in the second step¹⁵. In practice,
 123 we compute the new centroids μ by minimizing L_c using the stochastic gradient descent. A good choice of L_c is the soft
 124 assignment loss³⁵, which is the KL divergence of empirical clustering assignment distribution Q from a target distribution P .

125 Given an embedded point h_i and a centroid μ_j , Q is defined as Student's t -distribution $q_{ij} = \frac{(1 + \|h_i - \mu_j\|^2)^{-1}}{\sum_{j'} (1 + \|h_i - \mu_{j'}\|^2)^{-1}}$. An ideal target
126 distribution should have the following properties: (1) improve cluster purity, (2) put more emphasis on data points assigned
127 with high confidence, and (3) prevent large clusters from distorting the hidden feature space. In experiments, we choose P as
128 $P_{ij} = \frac{q_{ij}^2 / \sum_i q_{ij}}{\sum_{j'} q_{i,j'}^2 / \sum_i q_{i,j'}}$.

129 Evaluation metric

Clustering results are measured by Normalized Mutual Information (NMI)³⁶. Given the knowledge of the ground truth class assignments U and our clustering algorithm assignment V on n data points, NMI measures the agreement of the two assignment, ignoring permutations. NMI is defined as

$$\text{NMI}(U, V) = \frac{1}{\text{mean}(H(U), H(V))} \sum_{i=1}^{|U|} \sum_{j=1}^{|V|} \frac{|U_i \cap V_j|}{N} \log \left(\frac{n |U_i \cap V_j|}{|U_i| |V_j|} \right),$$

130 where $H(U) = -\sum_{i=1}^{|U|} \frac{|U_i|}{n} \log \left(\frac{|U_i|}{n} \right)$ is the entropy.

131 Trajectory inference results are measured by Kendall correlation coefficient. We define an order among the set of
132 observations $(x_1, y_1), (x_2, y_2), \dots, (x_n, y_n)$: any pair of observations (x_i, y_i) and (x_j, y_j) , where $i < j$ are said to be concordant
133 if either both $x_i > x_j$ and $y_i > y_j$ hold or both $x_i < x_j$ and $y_i < y_j$ hold; otherwise they are said to be discordant. Denote the
134 number of concordant pairs as N_{conco} and the number of discordant pairs as N_{discon} , Kendall correlation coefficient is defined as

$$\tau = \frac{2(N_{conco} - N_{discon})}{n(n-1)}.$$

135 Data simulation

136 We simulated five scRNA-seq datasets using Splatter R package (data1, data3, and data4) and PROSSTT Python package (data2
137 and data5). The cells in data1 and data5 are in the linear distribution along the developmental trajectory. The cells in data2
138 have a skewed distribution where cells concentrate at the center of each branch. The cells in data3 and data4 are in distinct
139 clusters with moderate and small cluster differences, respectively. All datasets have 2000 cells and 5000 genes. Data1, data2,
140 data3, and data4 were simulated for scenario1 to scenario4 for data visualization. Data5, data2, data3, and data4 are used for
141 the evaluation of scGAE on trajectory inference and cell clustering tasks.

142 Data preprocessing

143 The scRNA-seq data preprocessing was conducted using scTransform³⁷ in The Seurat package³⁸. The pre-processed count
144 matrix was used to construct the single-cell graph, where the nodes represent cells, and the edges represent the relationships
145 between cells. The cell graph is built by the K-nearest neighbor (KNN) algorithm³⁹ in the Scikit-learn Python package⁴⁰. The
146 default K is predefined as 35 in this study and adjusted according to the datasets in our experiments. The generated adjacency
147 matrix is a 0-1 matrix, where 1 represents being connected, and 0 represents no connection.

148 Empirical scRNA-seq data

149 We analyzed two different scRNA-seq datasets, namely HSPCs data and pancreatic cells data. HSPCs data and pancreatic
150 cells data represent cells showing lineages relationship and cells showing distinct clusters, respectively. The HSPCs data are
151 single-cell transcriptome data of FACS sorted CD34+ cells from human bone marrow mononuclear cells, accessible in the
152 national genomics data center (HRA000084) and described in our previous study⁵. The pancreases cells data contains 10,000
153 single-cell transcriptomes with 14 distinct cell clusters, download from GEO (GSE84133)²⁶.

154 Competitive methods

155 Seven competitive methods, namely scDeepCluster, DCA, SCVI, PCA, Ivis, SAUCIE, and PHATE, were compared with
156 scGAE. Among these methods, scDeepCluster, DCA, SCVI, Ivis, and SAUCIE are deep learning based and showed the greatest
157 potential. These methods usually generate hidden variables for downstream analysis, including visualization, clustering, and
158 trajectory inference. The raw count matrix was used as input for DCA, SCVI, and scDeepCluster. For methods that take
159 normalized data as input (scGAE, SAUCIE, PCA, Ivis, and PHATE), scTransform was used for data preprocessing. Each
160 software was run following its manual and with default parameters. For DCA, PCA was conducted to reduce the DCA-denoised
161 data to 32 PCs. For SAUCIE and Ivis, PCA reduced the preprocessed data to 100 PCs and 50 PCs, respectively. Ivis, SAUCIE,
162 and PHATE directly generate the 2-dimensional embeddings. The cell clustering and trajectory inference were performed on

163 the two-dimensional embeddings. Both scGAE and PCA embedded simulated data to 10 dimensions and embedded empirical
164 data to 20 dimensions due to the complex structure of the empirical data.

165 References

- 166 1. van der Maaten, L. & Hinton, G. Visualizing data using t-SNE. *J. Mach. Learn. Res.* **9**, 2579–2605 (2008).
- 167 2. Jaitin, D. A. *et al.* Massively parallel single-cell rna-seq for marker-free decomposition of tissues into cell types. *Science*
168 **343**, 776–779 (2014).
- 169 3. Klein, A. M. *et al.* Droplet barcoding for single-cell transcriptomics applied to embryonic stem cells. *Cell* **161**, 1187–1201
170 (2015).
- 171 4. Macosko, E. Z. *et al.* Highly parallel genome-wide expression profiling of individual cells using nanoliter droplets. *Cell*
172 **161**, 1202–1214 (2015).
- 173 5. Qin, P. *et al.* Integrated decoding hematopoiesis and leukemogenesis using single-cell sequencing and its medical
174 implication. *Cell discovery* **7**, 1–17 (2021).
- 175 6. Shapiro, E., Biezuner, T. & Linnarsson, S. Single-cell sequencing-based technologies will revolutionize whole-organism
176 science. *Nat. Rev. Genet.* **14**, 618–630 (2013).
- 177 7. Eraslan, G., Simon, L. M., Mircea, M., Mueller, N. S. & Theis, F. J. Single-cell rna-seq denoising using a deep count
178 autoencoder. *Nat. communications* **10**, 1–14 (2019).
- 179 8. Lopez, R., Regier, J., Cole, M. B., Jordan, M. I. & Yosef, N. Deep generative modeling for single-cell transcriptomics. *Nat.*
180 *methods* **15**, 1053–1058 (2018).
- 181 9. Tian, T., Wan, J., Song, Q. & Wei, Z. Clustering single-cell rna-seq data with a model-based deep learning approach. *Nat.*
182 *Mach. Intell.* **1**, 191–198 (2019).
- 183 10. Moon, K. R. *et al.* Visualizing structure and transitions in high-dimensional biological data. *Nat. biotechnology* **37**,
184 1482–1492 (2019).
- 185 11. Amodio, M. *et al.* Exploring single-cell data with deep multitasking neural networks. *Nat. methods* 1–7 (2019).
- 186 12. Szubert, B., Cole, J. E., Monaco, C. & Drozdov, I. Structure-preserving visualisation of high dimensional single-cell
187 datasets. *Sci. reports* **9**, 1–10 (2019).
- 188 13. Kipf, T. N. & Welling, M. Variational graph auto-encoders. *In NIPS Work. on Bayesian Deep. Learn.* (2016).
- 189 14. Veličković, P. *et al.* Graph attention networks. *Int. Conf. on Learn. Represent.* (2018).
- 190 15. Min, E. *et al.* A survey of clustering with deep learning: From the perspective of network architecture. *IEEE Access* **6**,
191 39501–39514 (2018).
- 192 16. Zappia, L., Phipson, B. & Oshlack, A. Splatter: simulation of single-cell rna sequencing data. *Genome biology* **18**, 1–15
193 (2017).
- 194 17. Papadopoulos, N., Gonzalo, P. R. & Söding, J. Prossitt: probabilistic simulation of single-cell rna-seq data for complex
195 differentiation processes. *Bioinformatics* **35**, 3517–3519 (2019).
- 196 18. Haghverdi, L., Büttner, M., Wolf, F. A., Buettner, F. & Theis, F. J. Diffusion pseudotime robustly reconstructs lineage
197 branching. *Nat. methods* **13**, 845 (2016).
- 198 19. Kendall, M. G. A new measure of rank correlation. *Biometrika* **30**, 81–93 (1938).
- 199 20. Velten, L. *et al.* Human haematopoietic stem cell lineage commitment is a continuous process. *Nat. cell biology* **19**,
200 271–281 (2017).
- 201 21. Buenrostro, J. D. *et al.* Integrated single-cell analysis maps the continuous regulatory landscape of human hematopoietic
202 differentiation. *Cell* **173**, 1535–1548 (2018).
- 203 22. Hay, S. B., Ferchen, K., Chetal, K., Grimes, H. L. & Salomonis, N. The human cell atlas bone marrow single-cell interactive
204 web portal. *Exp. hematology* **68**, 51–61 (2018).
- 205 23. Karamitros, D. *et al.* Single-cell analysis reveals the continuum of human lympho-myeloid progenitor cells. *Nat.*
206 *immunology* **19**, 85–97 (2018).
- 207 24. Tusi, B. K. *et al.* Population snapshots predict early haematopoietic and erythroid hierarchies. *Nature* **555**, 54–60 (2018).

- 208 **25.** Zheng, S., Papalexi, E., Butler, A., Stephenson, W. & Satija, R. Molecular transitions in early progenitors during human
209 cord blood hematopoiesis. *Mol. systems biology* **14**, e8041 (2018).
- 210 **26.** Baron, M. *et al.* A single-cell transcriptomic map of the human and mouse pancreas reveals inter-and intra-cell population
211 structure. *Cell systems* **3**, 346–360 (2016).
- 212 **27.** Bachem, M. G., Zhou, S., Buck, K., Schneiderhan, W. & Siech, M. Pancreatic stellate cells—role in pancreas cancer.
213 *Langenbeck's archives surgery* **393**, 891–900 (2008).
- 214 **28.** Lerique, S., Abitbol, J. L. & Karsai, M. Joint embedding of structure and features via graph convolutional networks. *Appl.*
215 *Netw. Sci.* **5**, 1–24 (2020).
- 216 **29.** Grattarola, D. & Alippi, C. Graph neural networks in tensorflow and keras with spektral. *Proc. The 37th Int. Conf. on*
217 *Mach. Learn.* (2020).
- 218 **30.** Kipf, T. N. & Welling, M. Semi-Supervised Classification with Graph Convolutional Networks. In *Proceedings of the 5th*
219 *International Conference on Learning Representations, ICLR '17* (2017).
- 220 **31.** Hamilton, W. L., Ying, R. & Leskovec, J. Inductive representation learning on large graphs. In *Proceedings of the 31st*
221 *International Conference on Neural Information Processing Systems, NIPS'17*, 1025–1035 (Curran Associates Inc., Red
222 Hook, NY, USA, 2017).
- 223 **32.** Du, J., Zhang, S., Wu, G., Moura, J. M. F. & Kar, S. Topology adaptive graph convolutional networks (2018).
- 224 **33.** Yang, B., Fu, X., Sidiropoulos, N. D. & Hong, M. Towards k-means-friendly spaces: Simultaneous deep learning and
225 clustering. In *international conference on machine learning*, 3861–3870 (PMLR, 2017).
- 226 **34.** Blondel, V. D., Guillaume, J.-L., Lambiotte, R. & Lefebvre, E. Fast unfolding of communities in large networks. *J. Stat.*
227 *Mech. Theory Exp.* **2008**, P10008, DOI: [10.1088/1742-5468/2008/10/p10008](https://doi.org/10.1088/1742-5468/2008/10/p10008) (2008).
- 228 **35.** Xie, J., Girshick, R. & Farhadi, A. Unsupervised deep embedding for clustering analysis. In *International conference on*
229 *machine learning*, 478–487 (PMLR, 2016).
- 230 **36.** Shannon, C. E. A mathematical theory of communication. *The Bell Syst. Tech. J.* **27**, 379–423, DOI: [10.1002/j.1538-7305.](https://doi.org/10.1002/j.1538-7305.1948.tb01338.x)
231 [1948.tb01338.x](https://doi.org/10.1002/j.1538-7305.1948.tb01338.x) (1948).
- 232 **37.** Hafemeister, C. & Satija, R. Normalization and variance stabilization of single-cell rna-seq data using regularized negative
233 binomial regression. *Genome biology* **20**, 1–15 (2019).
- 234 **38.** Stuart, T. *et al.* Comprehensive integration of single-cell data. *Cell* **177**, 1888–1902 (2019).
- 235 **39.** Peterson, L. E. K-nearest neighbor. *Scholarpedia* **4**, 1883 (2009).
- 236 **40.** Pedregosa, F. *et al.* Scikit-learn: Machine learning in python. *J. machine Learn. research* **12**, 2825–2830 (2011).

237 Acknowledgements

238 This study was supported by National Key R&D Program of China (2018YFC1004500), National Natural Science Foundation
239 of China (81872330, 31741077), the Science and Technology Innovation Commission of the Shenzhen Municipal Govern-
240 ment (JCYJ20170817111841427), the Shenzhen Science and Technology Program (KQTD20180411143432337), Center for
241 Computational Science and Engineering of Southern University of Science and Technology.

242 Author contributions statement

243 W.J. and Z.Z. conceived and designed the project. Z.L. and C.X. developed the algorithm, coded the program and performed
244 the data analysis. W.J. and Z.L. wrote the manuscript with inputs from all authors.

245 Additional information

246 **Accession codes** The code and software of scGAE are available on GitHub (<https://github.com/ZixiangLuo1161/scGAE>);
247 **Competing interests** The authors have declared that no competing interests exist.